Short Term Oxidation in HT-SEM of the Pt-containing TROPEA Single Crystal Ni-based Superalloy from 680 to 1000°C

S. Mathieu
stephane.mathieu@univ-lorraine.fr

Université de Lorraine, CNRS, IJL
R. Podor
ICSM, Univ Montpellier, CNRS, CEA, ENSCM, Site de Marcoule
M. Emo
Université de Lorraine, CNRS, IJL
L. Hunault
La Rochelle Université
M. Vilasi
Université de Lorraine, CNRS, IJL
J. Cormier
Institut Pprime, UPR CNRS 3346, ISAE-ENSMA
F. Pedraza
La Rochelle Université

Research Article

Keywords: Nickel-based superalloy, Oxidation, In Situ Observation

Posted Date: August 9th, 2024

DOI: https://doi.org/10.21203/rs.3.rs-4744310/v1

Additional Declarations: No competing interests reported.

Version of Record: A version of this preprint was published at High Temperature Corrosion of Materials on August 8th, 2024. See the published version at https://doi.org/10.1007/s11085-024-10272-9.

Short Term Oxidation in HT-SEM of the Pt-containing TROPEA Single Crystal Ni-based Superalloy from 680 to 1000°C

S. Mathieu[a*], R. Podor[b], M. Emo[a], L. Hunault[c], M. Vilasi[a], J. Cormier[d], F. Pedraza[c]

[a] Université de Lorraine, CNRS, IJL, Nancy, France
[b] ICSM, Univ Montpellier, CNRS, CEA, ENSCM, Site de Marcoule, Bagnols-sur-Cèze, France
[c] La Rochelle Université, LaSIE, La Rochelle, France
[d] Institut Pprime, UPR CNRS 3346, ISAE-ENSMA, Futuroscope-Chasseneuil, France
stephane.mathieu@univ-lorraine.fr; renaud.podor@cea.fr; melanie.emo@univ-lorraine.fr; louis.hunault@univ-lr.fr; michel.vilasi@univ-lorraine.fr; jonathan.cormier@ensma.fr; fernando.pedraza@univ-lr.fr
*corresponding author

Keywords. Nickel-based superalloy, Oxidation, In Situ Observation

Abstract. Short-time oxidation of the Ni-based TROPEA single-crystal superalloy was implemented to determine the nature and quantities of transient oxides in the 680-1000°C temperature range. Experiments were carried out in situ in the SEM with reduced air pressure (150 Pa, $P_{O_2} \sim 31.5$ Pa) compared to atmospheric conditions (10^5 Pa, $P_{O_2} \sim 2.1\ 10^4$ Pa). TEM characterization after oxidation showed the complexity of the oxidation products developed. Aluminum underwent internal oxidation between 680 and 1000°C. During the limited duration of oxidation, the TROPEA alloy only formed a continuous alumina layer at 1000°C. At 680 and 850°C, the low diffusion rate and small amount of Al in the Ni-based single crystal led to the formation of a significant amount of transient oxides such as (Ni,Co)O, compared to the desired chromia or alumina protective oxides. The lower the temperature, the smaller the size of the internal Al_2O_3 precipitates and the larger the transient oxide crystals, which would lower the resistance of TROPEA to Type II hot corrosion. In contrast after a transient period shorter than 22 hours, during which multiple transient oxide developed, the oxidation resistance would be ensured at 1000°C by the formation of a continuous Al_2O_3 scale.

1- Introduction

Current and future environmental concerns are forcing aircraft engine manufacturers to improve the efficiency of their turbojet engines. The most direct and effective way to do this is to increase the temperature of the combustion chamber, which in turn leads to an overall increase in the operating temperature of many engine components. To this end, a new generation of turbine blade alloys capable of withstanding higher temperatures than current alloys is continually being developed for high-pressure turbine blades. The need for ever-higher mechanical strength at high temperatures has led to the addition of Mo, W, Ta and Re to the composition of Ni-based superalloys, generally at the detriment of the elements Al and Cr, which are very useful for environmental resistance. Consequently, coatings based on β-NiPtAl, Pt-modified γ-Ni + γ'-Ni_3Al [1] or MCrAlY (M = Co or/and Ni) [2] are generally used to supply the required environmental resistance of Ni based single-crystal (SX) superalloys. Nevertheless, accurate knowledge of the intrinsic oxidation resistance of the uncoated alloy is necessary for a number of reasons: in the case of cracking or spalling of the coating, in places where the coating is missing (inside the blades for example [3]) or in cases where these alloys would be used uncoated.

One of the new Ni based superalloy is the platinum-containing TROPEA SX [4], which has been developed on the basis of the composition of the second-generation CMSX4 superalloy (Table 1). The addition of a low Pt content (0.6% at.) to substitute for the traditional refractory element Re ensures the stability of the γ' phase up to a temperature close to the solvus, hence improving mechanical properties at ultra-high temperature [4,5]. Indeed Rame *et al.* [4] reported that the TROPEA alloy exhibited excellent fatigue properties at 1200°C, creep strength and high yield stress similar to 2nd and 3rd generation superalloys. With Pt and a higher Ta content, the TROPEA alloy could be of interest respectively, under oxidizing conditions or in a corrosive atmosphere, as reported by Chang [6] and Fryburg [7].

With growth rates controlled by solid-state diffusion through α-Al_2O_3 layer, the degradation of Ni-based SX superalloys by oxidation in the medium-temperature range 700-900°C remains moderate in practice. This is probably why only few studies focused on the oxidation behaviour of γ/γ' Ni-base single crystal superalloys at temperature below 850°C. Nevertheless, Perez *et al.*[3] reported a very long transient period for the single crystal AM1 superalloy, associated with a high oxidation rate before the formation of a low growing rate of protective alumina scale. Conversely, corrosion accelerated by deposits, once initiated, can propagate rapidly and contribute to the degradation of the alloy's mechanical properties even at low temperatures [8,9]. The onset of hot corrosion [10,11,12] involves acidic or basic fluxing of the protective oxides; *i.e.* dissolution of the protective layer in a molten electrolyte. The presence of the liquid phase results from the interaction of SO_3 contained in the gas phase, with transient oxides such as NiO, CoO, Fe_2O_3 [13,14,15] in the presence of sulfate-based deposits. For all these reasons it was critical to identify the oxides forming at the surface of Ni-based superalloys in air, here on the TROPEA alloy, in the 650-700°C temperature range, corresponding to the Type II hot corrosion domain, and also 850-900°C, *i.e.* in the Type I hot corrosion domain [10] but also at higher temperatures, where "pure" oxidation takes the lead. For this purpose, oxidation was carried out in-situ in the scanning electron microscope at 680°C – 850°C – 1000°C.

2- Material and methods

The TROPEA alloy was manufactured by cold crucible induction melting from pure elements at the Safran Aircraft Engines foundry (France) using the conventional Bridgman process [4]. The samples were solution-treated for 24 h at 1300°C, quenched in air and then subjected to two precipitation heat treatments: the first lasting 4 hours at 1100°C followed by quenching in air, the second lasting 16 hours at 870°C also followed by quenching in air. The TROPEA alloy contains 75% of γ' phase after this sequence of heat treatments. More details regarding the alloy's microstructure can be found in [4]. The final chemical composition of TROPEA was measured by inductively coupled plasma atomic emission spectroscopy (ICP-AES). The composition is given in Table 1 along with that of CMSX-4 for comparison.

Table 1: Nominal compositions of TROPEA [4] and CMSX-4 [9] (in wt%)

	Ni	Co	Cr	Ti	Mo	Pt	Re	W	Ta	Hf	Al	S (ppm)
TROPEA	Bal.	9.0	6.5	1.0	0.6	2	1.0	6.0	9.0	0.1	6.5	6.9
CMSX-4	Bal.	9.7	6.4	1.1	0.6	/	2.9	6.4	6.5	/	5.8	~2

In situ SEM oxidation experiments were carried out in an environmental scanning electron microscope (ESEM, ThermoFicher Quattro S) equipped with a modified Thermofisher 1400°C heating stage. The main interest was to follow the evolution of the oxide scale growth at temperature, but also during cooling, and then to take FIB lamella on the same zone as the ones observed in the SEM. Prior to the experiment, cross-sections were polished with 1200 to 4000 grade SiC papers, then with a diamond solution (1 µm) and with a 0.1 µm colloidal silica suspension. SEM images were recorded with a GSED detector (Gaseous Secondary Electron Detector [16]) at an acceleration voltage of 15 kV. Samples were heated to the temperature of the experiment (680 - 850 and 1000°C respectively) at a rate of 25-30 K.min-1. The experiments were carried out under 150 Pa of air in the SEM chamber. The working total pressure was imposed by the ESEM technical specification, not chosen. But as low P_{O_2} favor selective oxidation, we can be confident in the fact that if the transient oxide are observed in the reduced P_{O_2} atmosphere of the ESEM, they should also be present in air.

The furnace was equipped with a thermocouple placed under the sample, enabling precise measurement of the sample temperature [17]. Once the target temperatures was reached, the samples were held in an isothermal stage and images were recorded regularly at different magnifications (1000X, 8000X and 16000X) to record information at different scales. Frame times were adjusted according to the rate of the oxidation reaction.

After exposure, cross sections of the oxide layers were obtained by extracting from the oxidized samples thin lamellas with a dual focused ion beam (FIB) scanning electron microscope (Helios Nanolab 600i) using the in situ lift-out technique. Lamellas with a thickness of around 50 nm were prepared for each sample. The area of interest was chosen to observe, if possible, the region around the grain boundary as well as the region on top of a metal grain (close to the area observed by SEM (see supplementary materials). A high resolution transmission electron microscope (TEM) (JEOL ARM 200F-Cold FEG) with a spherical aberration probe corrector (Cs) was used for scanning transmission electron microscopy (STEM) observations (Point resolution was 0.083 nm in STEM mode). The TEM was operated at an accelerating voltage of 200 kV. Chemical analyses were carried out with an energy dispersive X-ray (EDX) spectrometer (SDD, JEOL Dry SD 30 GV) in STEM mode.

3- Results

The first stages of oxidation were monitored directly using ESEM. Fig. 1 shows an overview of the TROPEA surface before and after oxidation at 680 - 850 - 1000°C. The oxidation time is indicated on each image. At 680°C, the difference in oxidation rate of the γ and γ' phases led to the formation of a discontinuous oxide layer in thickness. In some areas, large crystals grew mainly from the γ phase matrix and covered the γ/γ'microstructure. Conversely, in other areas, the oxide layer was so thin that the typical γ/γ'microstructure can still be observed after experiment. For temperatures of 850°C and 1000°C, the difference in oxidation behaviour between the two phases was observed during heating (see Supplementary materials). However, at higher temperatures the oxidation rate was faster. As a result, more oxides were formed and the alloy's microstructure disappeared after just a few minutes' exposure. This led to a more homogenous, crystallised scale covering the entire surface at the end of the experiment. At 850 and 1000°C, the oxide layer was composed of crystals of similar contrast and morphology, most probably of the same composition. FIB lamellae were extracted from representative areas to highlight the nature of the oxides forming on the γ and γ' phases for all three temperatures.

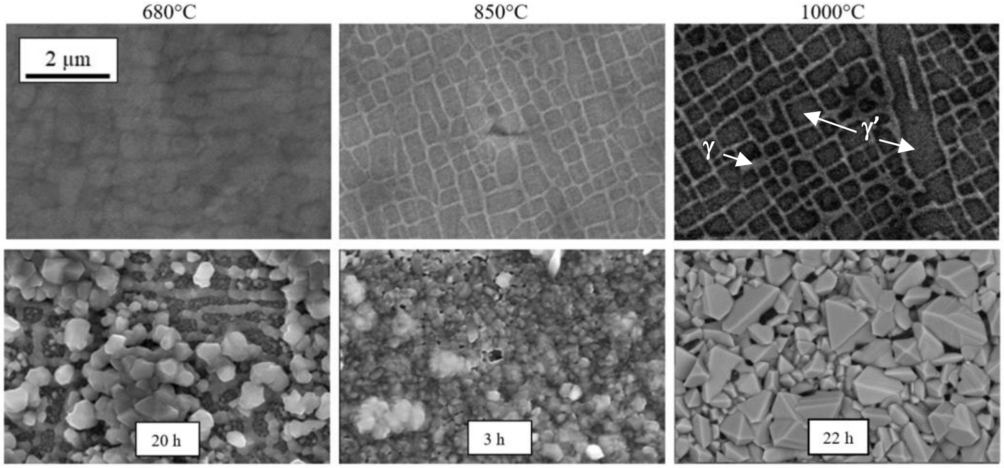

Fig. 1: Surface observations of TROPEA before (first pictures line) and after different times of oxidation (second line).

3.1. STEM characterization of TROPEA exposed to 680°C

Fig. 2 shows representative cross-section images of the TROPEA alloy after 20 hours of oxidation at 680°C in air, 150 Pa. The typical γ/γ' microstructure can still be observed after the experiment. Fig. 2b shows that only ~ 300 nm-thick subscale was modified during oxidation. However, in other areas of the lamellae, the impacted depth can reach 600 nm (data not shown). The γ' phase was much more impacted by oxidation than the γ matrix. The observations of the cross-section demonstrated the result of internal and external oxidation marked by a clear interface corresponding to the initial alloy surface (Figs. 2c and 2j). Ni and Co have formed a continuous external layer of large crystals of the (Ni,Co)O solid solution, with a NaCl ($Fm\overline{3}m\ ;a = 4.2$ Å) crystal structure (Fig. 2a). As observed by SEM, the size of some (Ni,Co)O crystals exceeded 500 nm in length, like the one in Fig. 2b. In the internal oxidation zone, nickel and cobalt concentrations have dramatically decreased. Considering the amount of (Ni,Co)O oxide at the top surface, it was clear that most of the Ni and Co forming these oxides came from the oxidation of the γ' phase. At the opposite, Al and Ta were internally oxidized within the initial γ' precipitates, where these elements were originally located (Fig. 2d and 2j). The distribution maps of Ta and Al show a barely visible enrichment near the initial alloy interface, indicating that these elements have nearly not moved during the 20 h oxidation at 680°C. On the contrary, oxygen penetrated into the alloy to a depth of 300 nm and was distributed in the same location as Al and Ta, hence suggesting internal oxidation of these elements (Fig. 2c). Both Cr- and Ti-containing oxides were located mainly near and on both sides of the initial interface (Fig. 2e and 2f). This indicated that Ti and Cr have slightly diffused towards the interface, unlike Al and Ta. A significant fraction of the Cr initially located in the γ' phase was also internally trapped, like Al and Ta, as oxygen diffused inwards. Macroscopically, Cr seemed to be more mobile than Al in the γ' phase. External Cr-rich oxides mainly developed at the top of the γ phase, which was initially richer in Cr than γ'. X-ray maps and EDS point analysis (data not shown here) shows that the grey crystals (see arrows in Fig. 2a) that have developed at the interface close to γ corridors (well identified on the Al distribution map) were Cr- and Ni- rich oxide, with a small amount of Co as well. The oxygen distribution map revealed a depletion in this element at the location of these crystals, indicating a lower oxygen-to-metal ratio than the surrounding oxides.

Consequently, these crystals should have a composition close to that of a spinel-type compound. The very small size of these crystals and their heterogeneous distribution in the lamella did not allow unambiguous identification of these crystals by electron diffraction. Around these Ni- and Cr- rich crystals, chromium was systematically enriched and only associated with oxygen. These chromium-rich regions of the layer must consist of chromia. Consequently, the oxide layer that has externally developed close to the initial interface consisted in a dotted line of chromia and spinel. As expected, since Pt was homogeneously distributed in the γ' phase, no evidence of its contribution to the oxidation mechanism was observed at this temperature.

3.2 STEM characterization of TROPEA exposed to 850°C

Fig. 3a shows a STEM image of the TROPEA alloy cross section after 3 hours exposure at 850°C in 150 Pa of air. The alloy was internally modified over 350-400 nm by oxidation. The distribution maps for Al and Ta again showed the location of the initial interface, as Al and mainly Ta diffused at a very short distance during oxidation. These elements were oxidized where they were initially located, i.e. within the γ' phase. Like at 680°C, some oxides developed inwardly and some others outwardly. The outer layer consisted of a continuous layer of (Ni,Co)O crystals with a lower fraction (100-150 nm thick) than at 680°C (> 500 nm thick). The (Ni,Co)O layer was physically separated from the Cr- and Ti-rich oxide layer situated just underneath, as if there were no adhesion between the two oxide layers. A high number of bright dots, probably of Pt were present on the internal interface of the (Ni,Co)O layer.

At 850°C, the Cr distribution map (Fig. 3d) shows a continuous distribution at the interface. Chromium was mainly located in a Co-containing spinel compound (probably $CoCr_2O_4$). Ni was absent from the spinel layer. Cr was also present in a Cr-rich oxide (most probably Cr_2O_3) that only formed locally in front of the γ corridors. This Cr-rich oxide did not form a continuous layer. These observations differed from those collected at 680°C, where a (Ni,Cr) spinel was mainly identified in front of the γ corridors. Titanium also accumulated at the interface close to chromia crystals, but not only since the $CoCr_2O_4$ spinel may contain some Ti (Fig. 3e). An enrichment of Al and Ti, forming a very thin layer (Fig. 3c) on top of Cr-containing oxides was also observed. This thin layer could be the former oxide that has grown outwards. A few amount of Al also appeared to be present in the $CoCr_2O_4$ spinel.

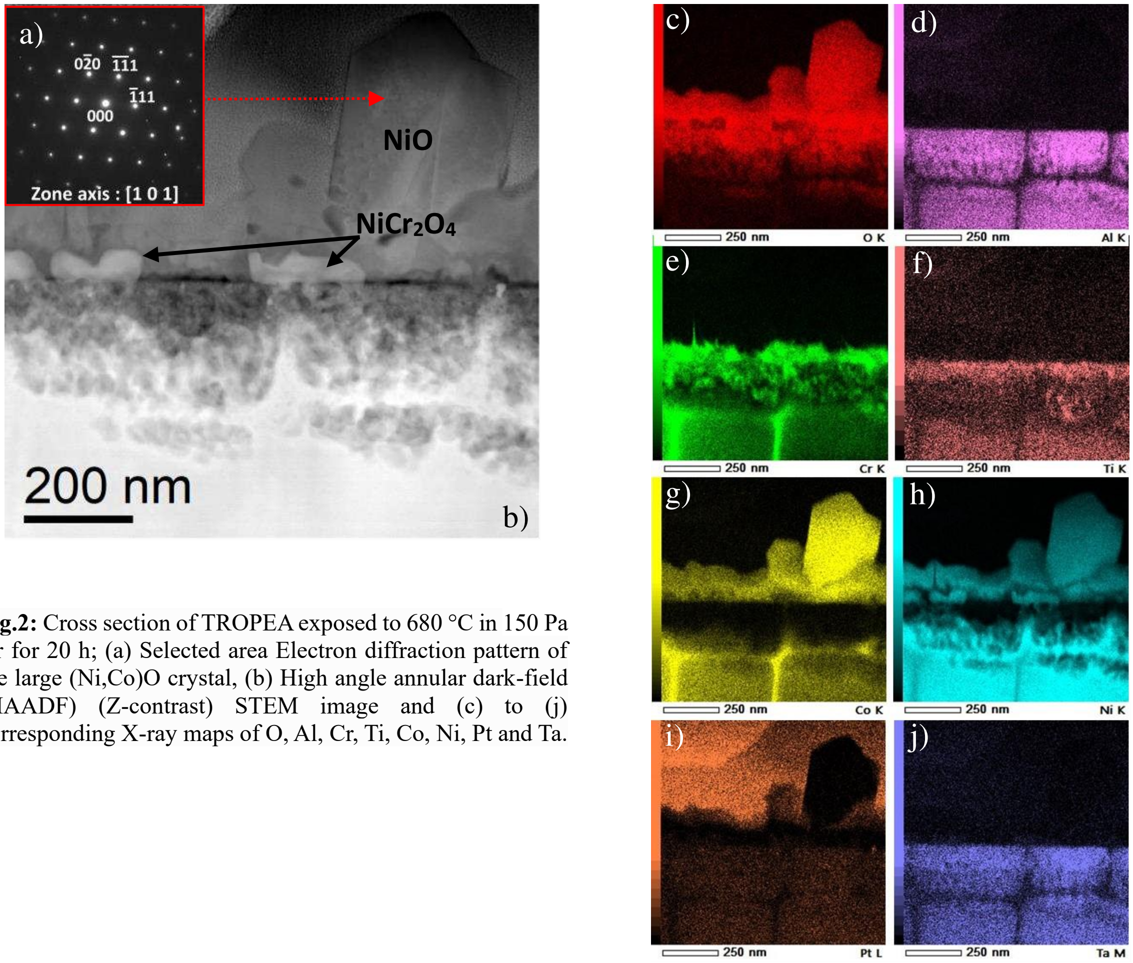

Fig.2: Cross section of TROPEA exposed to 680 °C in 150 Pa air for 20 h; (a) Selected area Electron diffraction pattern of the large (Ni,Co)O crystal, (b) High angle annular dark-field (HAADF) (Z-contrast) STEM image and (c) to (j) corresponding X-ray maps of O, Al, Cr, Ti, Co, Ni, Pt and Ta.

The main part of Al involved in the oxidation formed large, 100 nm-thick oxides, within the cuboidal γ'. These Al-rich oxides (most probably Al_2O_3) did not coalesce to form a protective layer after 3 hours of exposure at this temperature. The X-ray maps evidenced that the γ corridors are depleted in Cr and Co, but enriched in Ni, compared with the γ matrix unaffected by oxidation. The γ' crossing the initial surface has evolved to form a mixture of Al-, Ti-and Ta-rich oxides and non-oxidized metal residues. This evidenced that the oxygen partial pressure in this region was low enough to avoid the formation of the metallic oxides with the lowest free energy of formation, leading to their local enrichment. These were mainly Ni, Co and Cr. This may be due to residual Al that reduced the oxygen partial pressure or to the layer of Cr_2O_3 and spinel oxides that limited inward oxygen diffusion.. Finally, as diffusion should be enhanced at 850°C compare to 680°C, Al and Ti were depleted over 350-400 nm below the initial interface. As a result, the mixed γ/γ' microstructure evolved towards a Ni enriched γ layer. Interestingly, Co enrichment was not observed in the diffusion zone, indicating that Ni and Co behaved differently. The driving force for Co diffusion could be thus related to the formation of the Co-containing spinel layer.

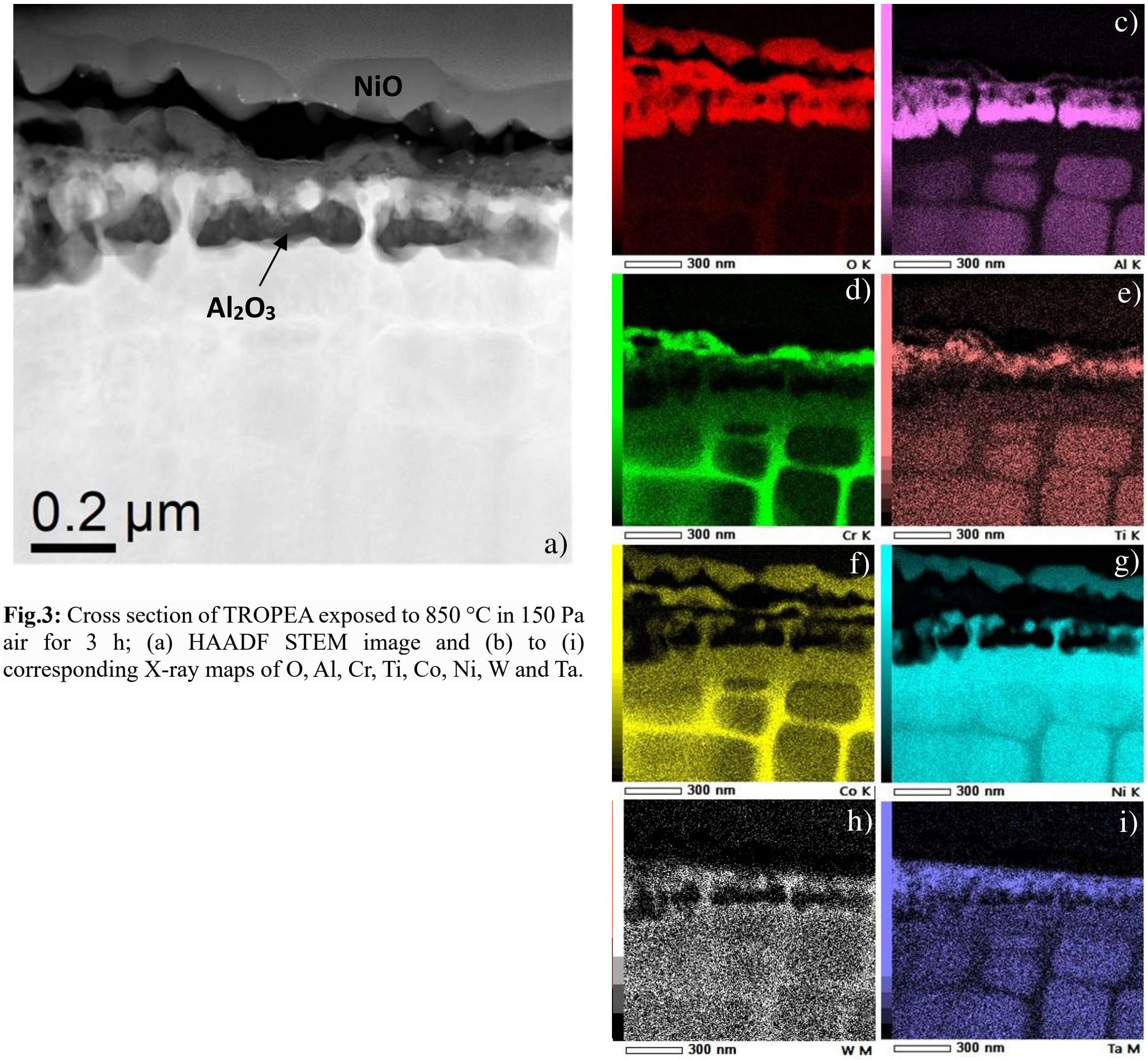

Fig.3: Cross section of TROPEA exposed to 850 °C in 150 Pa air for 3 h; (a) HAADF STEM image and (b) to (i) corresponding X-ray maps of O, Al, Cr, Ti, Co, Ni, W and Ta.

3.3 STEM characterization of TROPEA exposed to 1000°C

After 22 h at 1000°C (Fig. 4) in 150 Pa air, the oxidation of the TROPEA alloy was more pronounced. The whole oxides stack reached a thickness of 2.5 µm. The initial interface was no longer visible because of the strong modification occurring at the alloy surface. The γ/γ' microstructure was also less well defined than at 680 and 850°C. The affected diffusion zone has been estimated to more than 4 microns. Conversely, the oxides formed were better organized and large enough to be identified. As observed at 850°C, the outermost (Ni,Co)O layer (Fig. 4g, 4h) was physically separated from the Co and Ti-rich layer situated underneath (Fig. 4f, 4g). Only a few bridges ensured the adhesion of the outer (Ni,Co)O layer to the inner Co,Ti-rich oxide layer.

A dense and continuous layer of chromia was observed as part of the layer stack. The location of the Cr_2O_3 layer is obvious in Fig. 4g: it corresponds in the Co X-ray map to the dark layer situated between the two Co-rich oxide layers. The internal oxide layer appeared to be Al_2O_3 (Fig. 4d) with pores forming at the interface with the upper Ta and Ti-rich scale. To summarize, the successive oxide layers identified by EDS from the outer part of the oxide layer towards the parent alloy were: (Ni,Co)O – $CoTiO_4$ – (Ni,Co,Ti,Al)O – Cr_2O_3 – $(Co,Ni)Cr_2O_4$ – $TaTiO_4$ – Al_2O_3. Although the energies associated with the Ta Mβ and W Mα X-rays were close (1.766 keV and 1.775 keV resp.), it was possible to observe a few isolated nodules of W-rich oxide between the alumina and $TaTiO_4$ layers. In this area of low oxygen partial pressure, tungsten oxides such as WO_2 were thermodynamically expected. Platinum dots were observed in almost all oxide layers, with the exception of the outer (Ni,Co)O layer. It was not possible to characterize the presence of Pt in the Ta-rich layer due to the close energy of Pt Lα and Ta Lβ (9.441 keV and 9.341 keV resp.).

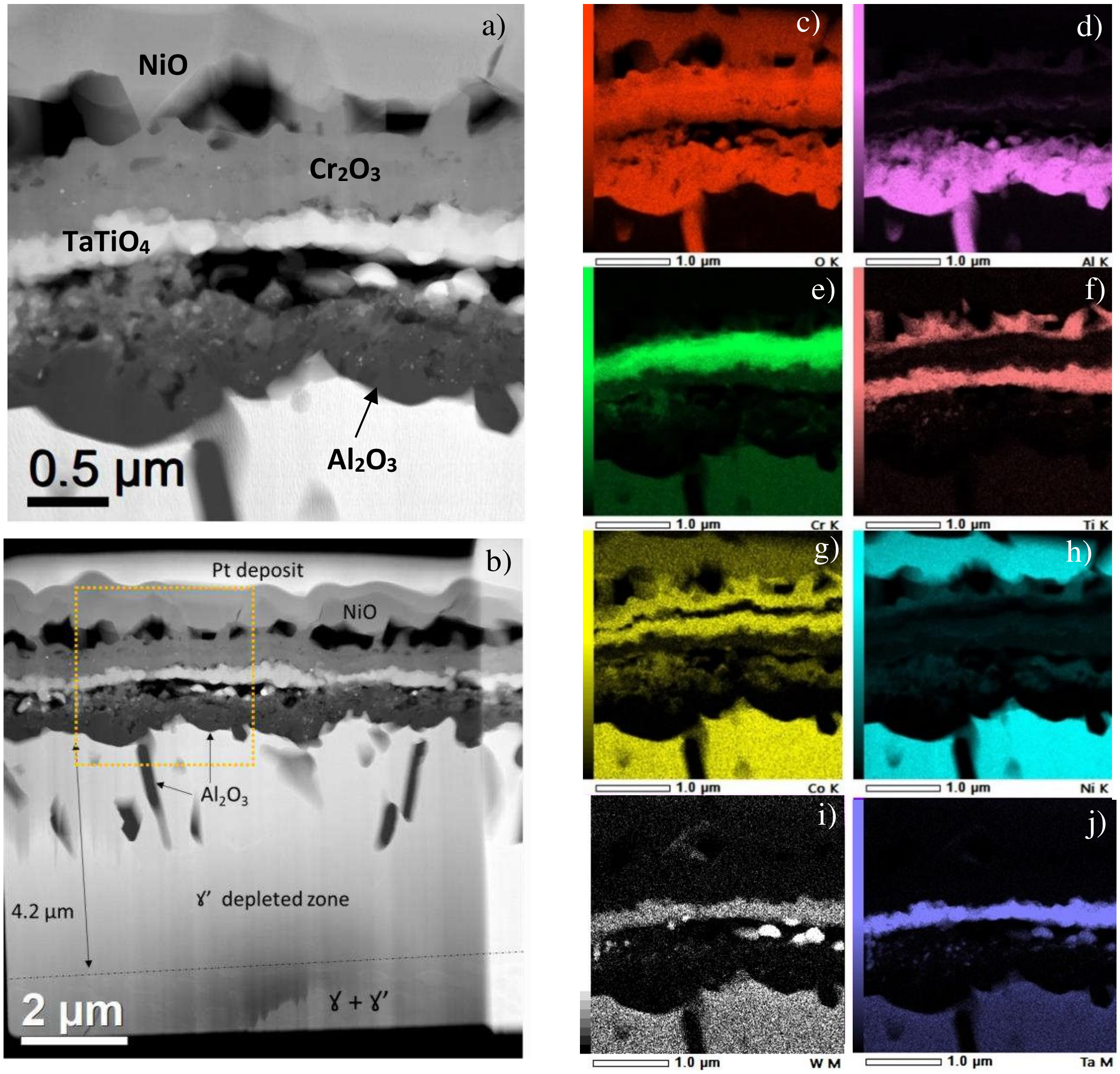

Fig.4: Cross section of TROPEA exposed to 1000 °C in 150 Pa air for 22 h; (a) and (b) HAADF STEM images and (c) to (j) corresponding X-ray maps of O, Al, Cr, Ti, Co, Ni, W and Ta.

4 Discussion

In-situ oxidation experiments were carried out using a scanning electron microscope (SEM) at 680 °C – 850 °C – 1000 °C in 150 Pa air in view of evaluating the ability of the TROPEA alloy to form a continuous and protective alumina or chromia scale at each temperature, to assess the nature and amount of the transient oxides and to determine the oxidation mechanism of this γ/γ' Ni-base single crystal superalloy. The main interest was to follow the growing oxide scale with temperature (see supplementary materials), but also during cooling; then to collect FIB lamella on the observed zones in the SEM. Of course, such kind of experiments might have been done in air without SEM, but in this case one can never be really sure that a part of the scale had not spalled during handling. The conditions employed in the SEM should favor the selective formation of protective alumina and chromium oxides, as i) the oxygen partial pressure (P_{O_2}) was reduced (~30 Pa), generally favoring the most stable oxide from a free energy point of view and ii) rapid heating (30 K/min) should reduce the quantity of transient oxides and improve resistance to oxidation.

Regardless of the location, *i.e.* either at the surface of γ or γ' phases, the SEM observations evidenced that the P_{O_2} in the SEM was sufficiently high at all temperatures to allow the formation of nickel and cobalt oxides. These were the main oxides to develop externally at 680 °C and 850 °C. (Ni,Co)O crystals with NaCl structure were identified on the upper surface of all samples. The volume fraction of the (Ni,Co)O mixed oxide relative to other oxides decreased with increasing temperature. This was particularly obvious at 680°C where these external oxides formed large crystals reaching 500 nm length in some areas after 20 h of exposure. Considering for discussion the parabolic constant of NiO formation on pure Ni determined by Peraldi *et al.* ($k_p = 10^{-11}\ g^2.cm^{-4}.s^{-1}$) [18] at 700°C for NiO layers lower than 5 µm thickness, the expected NiO thickness can be estimated to 580 nm. Consequently, the NiO growth from the TROPEA alloy at 680°C does not appear to be limited by the presence of the other metallic elements or oxides. Other oxides were observed in low amount and consisted of external oxides like chromia and $NiCr_2O_4$, the latter developing mainly at the top of the γ corridors. This situation was related to the oxidation behavior of γ' precipitates. Indeed, oxidation of these precipitates clearly occurred internally leading to Al- and Ta-oxide formation suggesting major oxygen inward diffusion. The initial interface remained perfectly flat despite the formation of these internal oxides, showing that this process occurred at constant volume. The involved mechanism could be the one known as the "Available Space Model (ASM)" [19], in which the process initiated with the formation of the external oxide (here NiO) at the oxide/environment interface through the outward cationic diffusion through the oxide layer. This induced the formation of metal vacancies at the metal/oxide interface and in the affected diffusion zone. The internal oxides thus grew within the available volume, facilitated by or in association with the rapid penetration of the oxidant to the metal/oxide interface through short-circuit diffusion paths. The scenario based on the expulsion of Ni because of the stresses that are generated by the expansion of volume during internal oxidation could also explain the observations [20,21,22]. Thus at 680°C, the TROPEA γ/γ' Ni-base SX superalloy only developed non-protective external Ni and Co oxides under current test conditions, and its oxidation rate was limited by diffusion of Ni cation through the NiO layer.

At 850°C, the mechanism was quite similar because the oxide externally and internally developed but the degradation was not so significant. The (Ni,Co)O thickness was lower than the one expected for pure Ni at this temperature, showing that the oxidation rate was limited by the formation of oxides with a lower growth rate than NiO. This was associated to the growth of other oxides like $CoCr_2O_4$ that were not present at 680°C, and to the enhanced growth of internal aluminum oxide. Indeed, larger domains of alumina developed within γ' so that a discontinuous layer of alumina formed. This alumina layer should reduce the inward diffusion of oxygen by reducing the diffusion cross section. With a lower P_{O_2} value at the metal-oxide interface, the oxidation of Ni can be to some extent limited with increasing oxidation time. Its strong enrichment in the external scale was noticeable in Fig.3h and in agreement with its affinity for oxygen, slightly higher than the affinity of oxygen for cobalt ($\Delta G^{\circ}_{850°C}(NiO) = -138\ kJ.mol^{-1}$ and $\Delta G^{\circ}_{850°C}(CoO) = -155\ kJ.mol^{-1}$[23]). Cobalt participated to the formation of the (Ni,Co)O external layer but Co contributed mainly to the formation of Co and Cr rich oxides, probably of spinel structure. Consequently, at 850°C, the formation of external cobalt and nickel oxides at the surface of TROPEA alloy was reduced compared to 680°C, but these oxides formed at 850°C.

At 1000°C, the fraction of (Ni,Co)O oxides formed relative to other oxides was the lowest. The successive layers identified from the outer part of the oxide layer towards the safe alloy were: (Ni,Co)O – $CoTiO_4$ – (Ni,Co,Ti,Al)O – Cr_2O_3 – $(Co,Ni)Cr_2O_4$ – $TaTiO_4$ – Al_2O_3. At this temperature, a continuous alumina scale of 500 nm on average formed at the metal-oxide interface under our testing conditions. Ni, Co and Cr concentrations below the Al_2O_3 scale were close to those expected in the initial alloy composition, showing that the P_{O_2} was low enough to limit their oxidation and that Al selectively oxidized. All oxides situated beyond the alumina layer were the result of the transient period required to form the alumina layer at the surface of the TROPEA alloy.

Concerning Pt, small dots of metallic platinum were observed. Pt is known to improve the efficiency of NiAl and γ/γ' diffusion coatings as it limits void formation at the oxide/scale coating interface, the diffusion of detrimental refractory elements to the gas/coating interface and also reduces the activity of Al in the coating, leading to an Al uphill diffusion from the superalloy towards the Pt-rich surface [24,25,26,27,28]. However, Pt content reached more than 5-6 %at. and 18-19%at. in the case of β-NiPtAl and γ/γ' diffusion coatings respectively [29]. The TROPEA alloy only contained 0.6%at. Pt. Therefore, the influence of Pt on the oxidation mechanism was not evidenced in this work. This requires further analysis including a comparison with the oxidation behavior of CMSX4, an alloy with a very similar composition but free of Pt.

All observations evidenced that whatever the temperature, Al and Ta oxidized internally and Ni and Co externally. As mentioned in the introduction, the formation of high amounts of Ni and Co oxides at 680 and 850°C on the surface of the Ni-based superalloys, and TROPEA for the present study, can be a real issue. Indeed, many authors [13,14,15] have shown that these oxides are prone to sulfation in air containing SO_2/SO_3 or when sulfate deposits are present. The sulfation reaction of NiO and/or CoO is a requisite for the formation of a liquid phase, which would be responsible for a very high corrosion rate associated with type II hot corrosion.

Conclusion

The TROPEA nickel-based single crystal superalloy was designed for high-pressure turbine blades. It was therefore not really surprising that this alloy exhibited poor resistance to oxidation in air in the low temperature range investigated here (680, 850°C). Oxidation can be described according to internal and external oxidation at 680°C and

850°C as clearly demonstrated by STEM. External Ni and Co oxides developed on nickel-based TROPEA superalloy. Conversely, Al and Ta oxidized internally within the initial γ' precipitates. At 680°C, a temperature within the range of the Type II hot corrosion, NiO growth was not hindered after 20 h of oxidation in the SEM environment. At 1000°C, transient oxides as well as Ta and Ti oxides were identified, but a continuous alumina layer developed at the interface with the alloy, likely ensuring protection against "pure" oxidation at high temperatures. In contrast, the formation of the transient Ni and Co oxides at low temperatures may be a severe issue for the resistance to type II hot corrosion of TROPEA but also for Ni-based SX superalloys of similar composition.

Acknowledgements

The authors acknowledge the French National Agency for Research for funding the ANR project ALUPLAT (ANR-21-CE08-0013).

Declaration of Conflicts of interest

The authors declare that they have no known competing financial interests or personal relationships that could have appeared to influence the work reported in this paper.

References

---

1. Xiao Q, Huang Q, Yang L, et al., *Corrosion Science* 2022;208:110638
2. Raffaitin A, Monceau D, Andrieu E, Crabos F, *Acta Materialia* 2006;54:4473–4487
3. Perez T, Monceau D, Desgranges C, *Corrosion Science* 2022;206:110485
4. Rame J, Utada S, Bortoluci Ormastroni LM, et al., Platinum-Containing New Generation Nickel-Based Superalloy for Single Crystalline Applications. In: Tin, S. et al. Superalloys 2020. The Minerals, Metals & Materials Series. Springer, Cham.
5. Van Sluytman JS et al., *Materials Science and Engineering* A, 2015;639:747-754
6. Chang JX, Wang D, Liu T, et al, *Corrosion Science* 2015; 98:585-591
7. Fryburg GC, Stearns CA, Kohl FJ, *J. Electrochem. Soc.* 1977;124:1147-1148
8. Brooking L, Gray S, et al., *International Journal of Fatigue* 2018;116:106-117
9. Yong Li, Cockings H, Mignanelli PM, et al., *Corrosion Science* 2022;207:110577
10. Goebel JA, Pettit FS, Goward GW, *Metallurgical Transactions* 1973;4: 261–278
11. Meier GH, *Oxidation of Metals* 98 (2021) 1-41.
12. Hu S, A review on molten sulfate salts induced hot corrosion, *Journal of Materials Science* 2021;90:243-254
13. Misra AK, Whittle DP, Worrell WL, Thermodynamics of Molten Sulfate Mixtures, *J. Electrochem. Soc.* 1982;129:1840–1845.
14. Luthra KL, Shores DA, *J. Electrochem. Soc.* 1980;127:2202.
15. Malacarne R, Mathieu S, et al., *Corrosion Science.* 2023;218:111186
16. Danilatos GD, *Micron and Microscopica Acta.* 1983;14:307–318.
17. Podor R, Pailhon D, Ravaux Y, Brau HP, *Microscopy and Microanalysis* 2015;21:307-312
18. Peraldi R, Monceau D, Jean S, Pieraggi B, *Materials at High Temperatures* 2003;20:649-655
19. F. Rouillard, G. Moine, L. Martinelli, J.C. Ruiz, Corrosion of 9Cr Steel in CO_2 at Intermediate Temperature I: Mechanism of Void-Induced Duplex Oxide Formation. *Oxid. Met.* 77, 27–55 (2012).
20. Schumann E, Schnotz G, Trumble KP, Rühle M, *Acta Metallurgica et Materialia*, 1992;6 :1311-1319,
21. Guruswamy S, Park SM, Hirth JP, Rapp RA, *Oxid. Met.* 1986;26:77–100
22. Kubacka D, Weiser M, Spiecker E, *Corrosion Science* 2021; 191:109744
23. Barin I and Knacke O, Thermochemical properties of inorganic substances. Springer-Verlag, 2nd ed (1991)
24. Liu C et al., *Acta Materialia* 2020;189:232-247.
25. Gleeson B et al. *Materials Science Forum* 2004;461-464:213-222
26. Pedraza F et al. *Surface and Coatings Technology* 2006;200:4032-4039
27. Sundman B et al. *Journal of phase equilibria and diffusion* 2009;30:602-607
28. Hou PY, Tolpygo VK, *Surface & Coatings Technology* 2007;202:623–627
29. Haynes J.A, Pint B.A., Zhang Y., Wright I.G. *Surface & Coatings Technology* 2007;202:730-734

Supplementary Files

This is a list of supplementary files associated with this preprint. Click to download.

- SuppMaterialsHTCM2.pptx